

Observation of the Exceptional Skin Effect on a Non-Hermitian Flat band

Dongyi Wang¹, Ruoyang Zhang², Chinghua Lee³, Kun Ding⁴, Guancong Ma⁵

1. Department of Physics, University of Hong Kong, Hong Kong, China
2. Department of Physics, The Hong Kong University of Science and Technology, Clear Water Bay, Kowloon, Hong Kong, China
3. Department of Physics, National University of Singapore, Singapore 117542, Singapore
4. Department of Physics, State Key Laboratory of Surface Physics, and Key Laboratory of Micro and Nano Photonic Structures (Ministry of Education), Fudan University, Shanghai 200438, China
5. Department of Physics, Hong Kong Baptist University, Kowloon Tong, Hong Kong, China

ABSTRACT:

Flat band and non-Hermitian are both significant conceptions in modern physics. In this study, we delve into the behaviours of flat bands in non-Hermitian systems, focusing on the interplay between the flat band and its dispersive counterparts, investigating the exceptional points (EPs) formed by them together, and the non-Hermitian skin effect (NHSE) on the flat band correspondingly generated, which we name as the exceptional skin effect (ESE). Employing non-Hermitian flat band under chiral/sublattice symmetry, where energy remains highly degenerate, we explore their unique properties. Unlike traditional NHSE which requires the enclosing of a non-zero area in the Bloch complex energy spectrum, the ESE on flat band can be generated with a Bloch complex energy spectrum consisting of one single point, i.e. enclosing no area. By analytically tuning non-Hermitian parameters, changes in the complex energy spectrum and Riemann surfaces are observed, revealing the formation of EPs through the hybridization of flat and dispersive bands while maintaining the dimension of the Hilbert subspace. Additionally, the wave functions of flat band exhibit ESE in specific parameter regions, contrary to the existing frameworks. Experimental validation is conducted using an elastic wave system with actively modulated non-Hermitian parameters, showcasing the impact on flat-band states and confirming the formation of ESE due to flat band-dispersive bands hybridization and correspondingly formed EPs. These results offer novel insights into non-Hermitian physics and present potential directions for further researches and applications in this field.

Introduction

Band theory is fundamental in various branches of modern physics¹, including solid physics², semiconductor physics³⁻⁵, photonics⁶⁻⁹, etc¹⁰. In band theory, waves propagating in periodic lattice are affected by Bragg scattering, thus energy bands are formed, the slope of which represent the group velocity of wave propagation⁶. Such group velocity is a determinant factor of materials' transportation properties. Among all kinds of energy bands, a specific type with perfect flatness protected by chiral/sublattice symmetry attracts much attention, that is the well-known flat band¹¹⁻¹⁵. With zero group velocity, wave and carriers exhibit special behaviours on flat bands: the extremely low mobility of carriers on the flat band is beneficial for the generation of superconducting pairs, which is crucial in researches on superconductivity³⁻⁵; the wave-functions of such flat bands are spatially localized on certain sites, forming compact localized states with highly degenerate energy levels^{8,13,14}, thus creates high-dimensional Hilbert subspace which is the physical basis for novel phenomena including topological braidings¹⁶⁻¹⁸, Thouless pumping^{19,20}, non-Abelian dynamics²¹⁻²³, etc.

However, current researches on flat bands and corresponding eigenstates are mostly limited to Hermitian cases^{10,11}. Over the past few years, non-Hermitian physics, which focuses on open systems allowing energy exchange with the environment, has emerged as a new frontier in physics²⁴⁻²⁶. Employing non-self-adjoint Hamiltonians with complex energy spectrum to capture non-Hermitian systems, scientists found a special kind of singular points formed by at least two merged levels, regarded as exceptional points (EPs)²⁷⁻²⁹, where the eigen states are mutually parallel. Non-Hermitian skin effect (NHSE) is another important phenomenon in non-Hermitian systems³⁰⁻³². With generally non-orthogonal properties, the wave functions of continuous spectra become localized at the boundaries, i.e. skin states are formed rather than bulk states under non-Hermitian conditions. Introducing non-Hermitian into a system with flat band while preserve the symmetry might induce novel phenomena, yet has not been precedently studied.

In this work, we establish a system where the flatness of certain bands is still safeguarded by chiral/sublattice symmetry under non-Hermitian circumstances, i.e. energy is still highly degenerated. Employing such system, we first analytically explore the properties of

the non-Hermitian flat bands: tune the non-Hermitian parameters, observe the changes correspondingly induced in the complex energy spectrum and Riemannian surfaces. Through derivations, it is verified that EPs can be formed by the hybridization of flat bands with dispersive bands for certain parameters, yet leaving the dimension of the Hilbert subspace uninfluenced. Additionally, a special kind of NHSE, which we name as exceptional skin effect (ESE), is found to affect the wave functions of flat bands in specific parameter regions, originated from hybridization and EPs formed by flat band together with dispersive bands, enclosing no area on the Bloch complex energy spectrum, contrary to existing theoretical frameworks³⁰. Next, we employ an elastic wave system where non-Hermitian parameters can be actively modulated with time to experimentally characterize the effects of non-Hermitian parameters on the flat-band states. By dynamically changing the parameters to induce different EPs in a four unit-cell system, it's observed in experiment that the flat-band eigenstates are influenced by ESE yet displaying different wave-function profiles, demonstrating the impact of hybridization with different dispersive bands. Similar phenomenon is further validated in a larger-size system consisting of twelve unit-cells. The experimental results align with theoretical predictions, confirming the formation of ESE on flat bands in the presence of flat band-dispersive bands hybridization and correspondingly formed EPs.

This study provides insights into the behaviour of flat bands in non-Hermitian systems and highlights the interplay between flat bands and dispersive bands in generating EPs and flat-band ESE. The findings in this work contribute to novel understandings of non-Hermitian physics, and offer potential avenues for further research in this field and future applications.

Results

Theoretical analysis of ESE on a non-Hermitian flat band

Through preliminary investigations, a non-Hermitian system is selected as the appropriate candidate as shown in Fig. 1 (a), which is composed by three-site unit cells and possesses a symmetry-protected flat band unaffected by non-Hermitian parameters. Such system can be captured by a Hamiltonian under periodic boundary condition (PBC):

$$H(k) = \begin{pmatrix} E_s & t_1 - \frac{\gamma_1}{2} + t_2 * e^{-ik} & t_2 - \frac{\gamma_2}{2} \\ t_1 + \frac{\gamma_1}{2} + t_2 * e^{ik} & E_s & 0 \\ t_2 + \frac{\gamma_2}{2} & 0 & E_s \end{pmatrix} \quad (1)$$

Where E_s denotes onsite energy of each site; $t_1 \pm \frac{\gamma_1}{2}$ denotes non-reciprocal intra-cell coupling between sites A and B, γ_1 capturing the strength of non-Hermitian parameter; t_2 denotes the reciprocal inter-cell coupling between sites A and B; $t_2 \pm \frac{\gamma_2}{2}$ denotes non-reciprocal intra-cell coupling between sites A and C, γ_2 capturing the strength of non-Hermitian parameter. The corresponding Hamiltonian in the open boundary condition (OBC) describing a system composed of N unit-cells denotes:

$$H_{\text{OBC}}^N = \sum_{n=1}^N \left[E_s (a_n^\dagger a_n + b_n^\dagger b_n + c_n^\dagger c_n) \left(t_1 + \frac{\gamma_1}{2} \right) b_n^\dagger a_n + \left(t_1 - \frac{\gamma_1}{2} \right) a_n^\dagger b_n + \left(t_2 + \frac{\gamma_2}{2} \right) c_n^\dagger a_n + \left(t_2 - \frac{\gamma_2}{2} \right) a_n^\dagger c_n \right] + \sum_{n=1}^{N-1} t_2 (a_{n+1}^\dagger b_n + b_n^\dagger a_{n+1}) \quad (2)$$

with a_n^\dagger , a_n ; b_n^\dagger , b_n ; c_n^\dagger , c_n denoting the creation and annihilation operators on the sublattices A, B, C in the n th unit cell, respectively. It's clear that H_{OBC}^N possesses sublattice symmetry:

$$\Gamma H_{\text{OBC}}^N \Gamma = -H_{\text{OBC}}^N \quad (3)$$

with $\Gamma = \begin{pmatrix} I_{N_+ \times N_+} & \\ & -I_{N_- \times N_-} \end{pmatrix}$, which protects a flat band in the system unaffected by non-Hermitian parameters, making it an appropriate candidate for further investigations.

We firstly investigate a four unit-cell system. Varying the non-Hermitian parameters γ_1 and γ_2 , the corresponding real and imaginary parts of the Bloch complex energy are shown

in Fig. 1 (b, c) respectively. It's clearly seen that the real parts for a pair of dispersive bands merge on to their flat band counterpart while the imaginary parts of them split on four specific parameter lines, thus EPs are supposed to be formed by the flat band and dispersive bands together. Six typical points are marked on the $\gamma_1 = 1.52$ intersection, with $\gamma_2 = 0.20$ [gray star], $\gamma_2 = 1.20$ [red star], $\gamma_2 = 1.57$ [blue star], $\gamma_2 = 1.99$ [green star], $\gamma_2 = 2.28$ [yellow star] and $\gamma_2 = 3.00$ [gray star], being a real energy band-gap open point, the four flat band-dispersive bands hybridized EPs, and an imaginary energy band-gap open point, respectively.

Fixing $\gamma_1 = 1.52$ and varying γ_2 , we take a closer look at the evolution of Bloch energy spectrum, Riemannian surfaces and corresponding GBZ when the non-Hermitian parameters vary. As shown in Fig.1 (d, j, g), according to the spectrum on complex Bloch energy plane, there are three typical points in the non-Hermitian parameter space, blue dots denoting PBC solutions and red dots denoting their OBC counterparts consisting of four unit-cells. The band gap opens on the real axis when $\gamma_2 = 0.20$ [Fig.1 (d)], closes for $\gamma_2 = 1.57$ [Fig.1 (g)], and re-opens on the imaginary axis when $\gamma_2 = 3.00$ [Fig.1 (j)]. As emphasized by the gray boxes, the Bloch energy spectrum for the flat-band always remains as one single point enclosing no area for both PBC and OBC throughout the variation of non-Hermitian parameters.

The corresponding Riemannian surfaces and GBZ solution β are also evaluated. The flat-band GBZ solution β_{FL} denoted by the red dots are firstly separated from their dispersive-band counterparts denoted by the blue dots on the Riemannian surfaces [Fig. 1 (e,f)] (corresponding to the gap-open condition); then evolve on the loops formed by the dispersive-band GBZ solutions, zipping up the real energy parts and unzipping their imaginary counterparts simultaneously when passing through different EPs in sequence [Fig. 1 (h,i)]; and eventually separate from their dispersive-band counterparts again [Fig. 1 (k,l)].

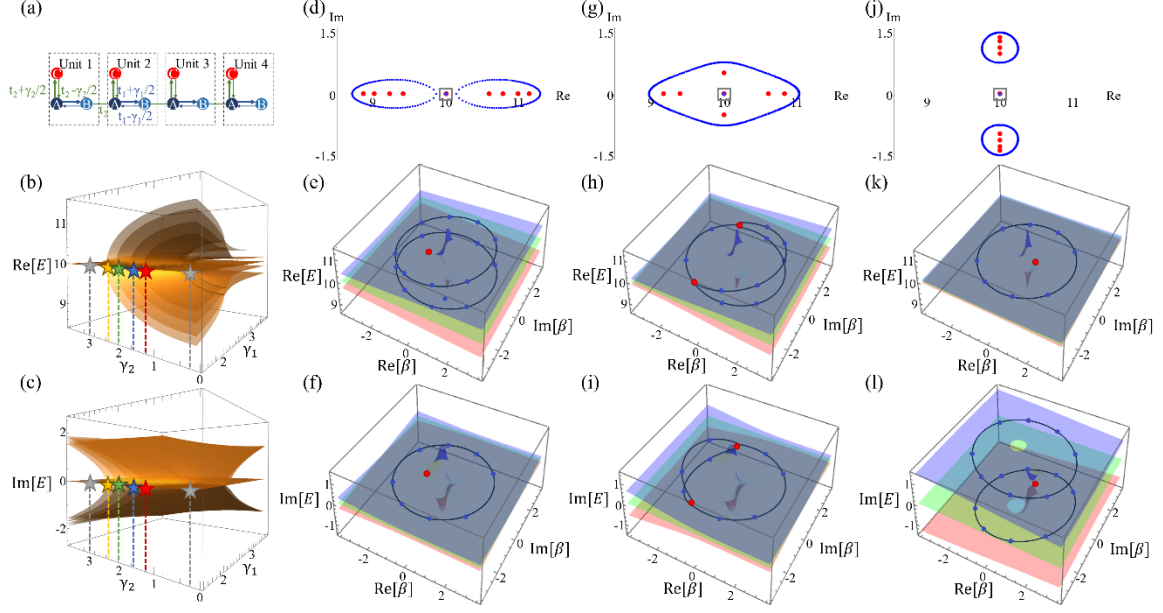


Fig.1 Schematics and theoretical analysis on a non-Hermitian flat band system with ESE. (a) Schematics of the non-Hermitian flat band system under OBC consisting of four unit-cells, A, B, C denoting different sublattices within each unit cell, $t_1 \pm \frac{\gamma_1}{2}$ denoting non-reciprocal intra-cell coupling between sites A and B, γ_1 capturing the strength of non-Hermitian parameter; t_2 denoting the reciprocal inter-cell coupling between sites A and B; $t_2 \pm \frac{\gamma_2}{2}$ denoting non-reciprocal intra-cell coupling between sites A and C, γ_2 capturing the strength of non-Hermitian parameter. The (b) real and (c) imaginary part of the eigen energy cut at the interface where $\gamma_1 = 1.52$ when varying the non-Hermitian parameters γ_1 and γ_2 , the six stars mark the parameter points $\gamma_2 = 3.00$ (gray), $\gamma_2 = 2.28$ (yellow), $\gamma_2 = 1.99$ (green), $\gamma_2 = 1.57$ (blue), $\gamma_2 = 1.20$ (red) and $\gamma_2 = 0.20$ (gray), from left to right, respectively. At the yellow, green, blue and red stars marked parameter points, real parts of two dispersive bands merge onto the flat band while the imaginary parts split from the flat band correspondingly, indicating the existence of EPs. Fix $\gamma_1 = 1.52$, the Bloch energy spectrum on the complex plane for (d) $\gamma_2 = 0.20$, (g) $\gamma_2 = 1.57$, (j) $\gamma_2 = 3.00$; blue dots denoting PBC solutions and red dots denoting their OBC counterparts containing 4 unit cells. The gray boxes mark the flat-band PBC and OBC spectrum, which is always one single point. Fix $\gamma_1 = 1.52$, the real part of the Riemannian surfaces and corresponding β solved by GBZ method for (e) $\gamma_2 = 0.20$, (h) $\gamma_2 = 1.57$, (k) $\gamma_2 = 3.00$; and the imaginary part of the Riemannian surfaces and corresponding β solved by GBZ method for (f) $\gamma_2 = 0.20$, (i) $\gamma_2 = 1.57$, (l) $\gamma_2 = 3.00$, blue dots denoting β_{DB} solutions for dispersive bands of a four-unit-cell system while red dots denoting their flat-band counterparts β_{FB} , solid lines marking the GBZ circle solved from larger system's dispersive bands.

The general condition for NHSE in 1D systems is enclosing a non-zero area in the Bloch complex energy spectrum; for non-Hermitian flat bands, as illustrated by the gray boxes in Fig.1 (d, g, j), the Bloch complex energy spectrum consists of one single point, which clearly encloses no area, i.e., non-Hermitian flat bands should exhibit no NHSE according to the existing theoretical framework. While as suggested by the fact that $\beta_{FL} > 1$ when the flat-band GBZ solution evolves on the loops formed by their dispersive-band counterpart, a special kind of NHSE should exist on the flat band, which is not induced by a loop enclosing certain area on the Bloch energy spectrum, but the hybridization between

the flat band and dispersive bands instead. We call it the exceptional skin effect (ESE). The evolution process with more parameter points in larger system can be found in Section 1 of Supplementary Information (SI).

Clearly, with no area enclosed on the energy spectrum, hybridization with the dispersive bands must be the critical reason for the ESE on the flat band, i.e., the EPs formed should be carefully investigated. Through simple symmetry analysis and analytical calculations [Section 2 in SI], no higher than $n + 1^{\text{th}}$ order EP can be generated when n dispersive bands merge onto the flat band, thus the generated EP are 3^{rd} order ones in this four unit-cell system with a pair of dispersive bands merging onto the flat band for each EP. By using the resultant for characteristic polynomials [Section 2 in SI], the four EP lines can be analytically solved in the 2D non-Hermitian parameter space as shown in Fig. 2 (a), being $\gamma_2 = f_1(\gamma_1)$, $\gamma_2 = f_2(\gamma_1)$, $\gamma_2 = f_3(\gamma_1)$, $\gamma_2 = f_4(\gamma_1)$, corresponding to the yellow, green, blue and red lines respectively. Setting $\gamma_1 = 1.52$ and four different γ_2 can be analytically found as EP parameters. At $\gamma_2 = 2.28, 1.99, 1.57, 1.20$, the wave function profiles of flat-band eigen states in the four-unit-cell OBC system are shown in Fig. 2 (e), colours of frames corresponding to differently coloured stars marking different non-Hermitian EP parameters in Fig. 2 (a). The ESE can be clearly observed for these flat-band eigen states at EPs; one thing to notice is that the wave functions are different for four EPs, since different pairs of dispersive-band states with different exponential decay rates fall onto the flat band in sequence, thus when the flat-band states forming EPs together with them are influenced by their NHSE, the ESE profiles also look different.

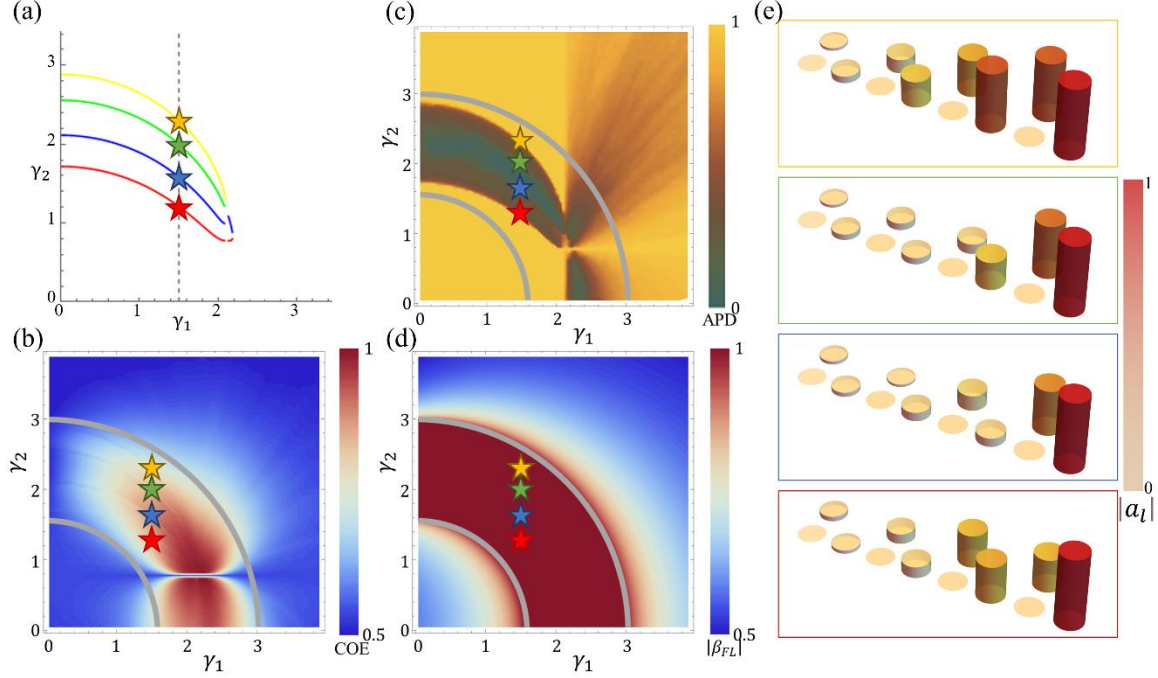


Fig.2 Analysis on EPs and flat-band ESE in a non-Hermitian flat band system. (a)The four EP lines analytically solved in the non-Hermitian parameter plane of the system, The yellow, green, blue and red lines denoting the EP lines: $\gamma_2 = f_1(\gamma_1)$, $\gamma_2 = f_2(\gamma_1)$, $\gamma_2 = f_3(\gamma_1)$, $\gamma_2 = f_4(\gamma_1)$, respectively. (b) The centre of energy (COE) variation diagram versus γ_1 , γ_2 ; (c) the average phase rigidity (APD) diagram versus γ_1 , γ_2 ; (d) the $|\beta_{FL}|$ for flat band solved analytically by Generalized Brillouin Zone (GBZ) method versus γ_1 , γ_2 , in a four-unit-cell system, the two gray lines denoting PBC gap-closed boundaries, below which a band gap is opened on the real part, and above which a band gap is opened on the imaginary part. (e) The wave-functions of the flat-band eigen states at EPs at the parameter points $\gamma_1 = 1.52, \gamma_2 = 2.28$ (yellow framed), $\gamma_1 = 1.52, \gamma_2 = 1.99$ (green framed), $\gamma_1 = 1.52, \gamma_2 = 1.57$ (blue framed) and $\gamma_1 = 1.52, \gamma_2 = 1.20$ (red framed), corresponding to the parameter points marked by the same-coloured stars in (a,b,c,d), i.e. different EPs.

To further estimate the hybridization process and the flat-band ESE correspondingly induced in the non-Hermitian parameter space, we define three different parameters. First, for an OBC system containing N unit cells, we define the average centre of energy for each eigen state on the flat band:

$$\text{COE} = \frac{\sum_{j=1}^N \left(\frac{\sum_{l=1}^{3N} l |a_l|^2}{3N} \right)}{N} \quad (4)$$

Where $\psi_0^j = \begin{pmatrix} a_1 \\ a_2 \\ \dots \\ a_l \\ \dots \\ a_{3N} \end{pmatrix}$ are the N flat-band eigen vectors, $j=[1,N]$; $l = [1,3N]$ labels $3N$

different positions in the 1D system. Thus, $\text{COE} = 0.5$ indicates even distributions among

different unit-cells, while COE close to 0 or 1 indicates strong NHSE towards the left or right side of the chain. As shown in Fig. 2 (b), COE is close to 1, i.e. ESE can be observed in the PBC gap closed area surrounded by the gray critical boundaries, even not at the exact EPs.

The average phase rigidity on the flat band is another quantity we employ:

$$\text{APD} = \frac{\sum_{j=1}^N (|r_j|)}{N}; \quad |r_j| = \left| \frac{\langle \tilde{\phi}_j^L | \tilde{\phi}_j^R \rangle}{\langle \tilde{\phi}_j^R | \tilde{\phi}_j^R \rangle} \right| \quad (5)$$

where $\langle \tilde{\phi}_j^L |, |\tilde{\phi}_j^R \rangle$ denote normalized biorthogonal left and right eigenvectors respectively, $j = [1, N]$ labels the flat-band eigen vectors, thus APD denotes the average value of all flat-band modes' phase rigidities. As Fig. 2 (c) demonstrates, for certain non-Hermitian parameter areas within the PBC gap-closed critical boundaries, phase rigidities vanish, suggesting the hybridization between flat band and dispersive bands.

The last parameter employed for ESE evaluation is $|\beta_{FL}|$ calculated for the flat band based on the generalized Brillouin zone (GBZ). Replacing the e^{ik} in the PBC Hamiltonian $H(k)$ with β , we can transfer $H(k)$ to $H(\beta)$:

$$H(\beta) = \begin{pmatrix} E_s & t_1 - \frac{\gamma_1}{2} + t_2 * \frac{1}{\beta} & -\frac{\gamma_2}{2} \\ t_1 + \frac{\gamma_1}{2} + t_2 * \beta & E_s & 0 \\ +\frac{\gamma_2}{2} & 0 & E_s \end{pmatrix} \quad (6)$$

For an OBC system containing N unit cells, $3N$ eigenvalues E_i , $i = 1 \dots 3N$ can be found. Solving the determinant $\det[H(\beta) - E_i * I_3] = 0$, the corresponding β can be solved, which are the aGBZ solutions. Further sorting β by absolute values $|\beta_1| \leq |\beta_2| \leq \dots \leq |\beta_{2M-1}| \leq |\beta_{2M}|$, the GBZ solutions can be obtained by selecting $|\beta_M| = |\beta_{M+1}|^{25}$. As shown in Fig 2 (d), the flat-band GBZ solution $|\beta_{FL}| > 1$ in the PBC gap closed region, suggesting probable ESE, which consist well with the COE and APD results. Results for larger system can be found in Section 3 of SI.

To conclude, through theoretical analysis, the underlying physical view of the flat-band ESE is pretty clear: the eigen-energy gap is firstly closed on the real axis then reopened on

the imaginary axis, and the flat-band eigen states form EPs with different dispersive-band states one pair by one pair when the non-Hermitian parameters vary, during the process of which the initially localized flat-band eigen states get influenced by the NHSE of their dispersive-band counterparts with different spatially-distributed profiles, thus ESEs with varied wave function profiles on the flat band is induced.

Experimental observation of ESE on a non-Hermitian flat band

To further verify the flat-band ESE induced by hybridization of flat band and dispersive bands, with non-Hermitian parameters dynamically modulated from zero to the gap-closed region where flat-band ESE is expected to happen, we experimentally observe this novel phenomenon in the elastic wave system with excitations at different positions.

We employ a brushless motor equipped with two perpendicular rotational arms³³, one of them is connected to two anchor points by tensioned springs to form a rotational oscillator, providing an on-site term E_s . All the oscillators are carefully modulated to obtain identical on-site terms in the Hermitian case, and divided into groups A, B, C, then connected via tensioned springs to form a 1D lattice, the connecting springs providing constant couplings t_1 and t_2 respectively, denoted by the blue and green lines as shown in Fig. 3 (a). Including also non-reciprocal couplings by programmed external actuation of the motors, non-Hermitian parameters γ_1, γ_2 can be freely modulated, thus the time evolution process from the original Hermitian point to a designated non-Hermitian point can be experimentally realized. All the corresponding parameters $E_s, t_1, t_2, \gamma_1, \gamma_2$ are retrieved from preliminary experiment by Green's function method.

We first experimentally capture the ESE behaviour near different EPs in a 4 unit-cell system as shown in Fig. 3(a), where the EP lines in the non-Hermitian parameter space can be analytically solved as demonstrated in the last section. Set the total evolution time to be $t_{\text{tot}} = 15\text{s}$, actively modulate the Non-Hermitian parameters from the Hermitian point ($\gamma_1 = \gamma_2 = 0$) to different non-Hermitian induced EPs $\gamma_1 = 1.52, \gamma_2 = 2.28, 1.99, 1.57, 1.20$ denoted by the yellow, green, blue and red stars on different EP lines respectively [Fig. 2(a)]. To presume adiabatic approximation, the non-Hermitian parameters are dynamically modulated as:

$$\gamma_1 = 1.52 * \text{Sin}\left[\frac{15(t-2*t_{\text{tot}}/5)\pi}{2*t_{\text{tot}}}\right]$$

$$\gamma_2 = \gamma_f * \text{Sin}\left[\frac{15(t-2*t_{\text{tot}}/5)\pi}{2*t_{\text{tot}}}\right]$$
(7)

$\gamma_f = 2.28, 1.99, 1.57, 1.20$ denoting the final values of γ_2 respectively, where the dynamics are governed by the time-dependent Schrödinger equation $H(t)|\psi_n(t)\rangle = \varepsilon_n(t)|\psi_n(t)\rangle$.

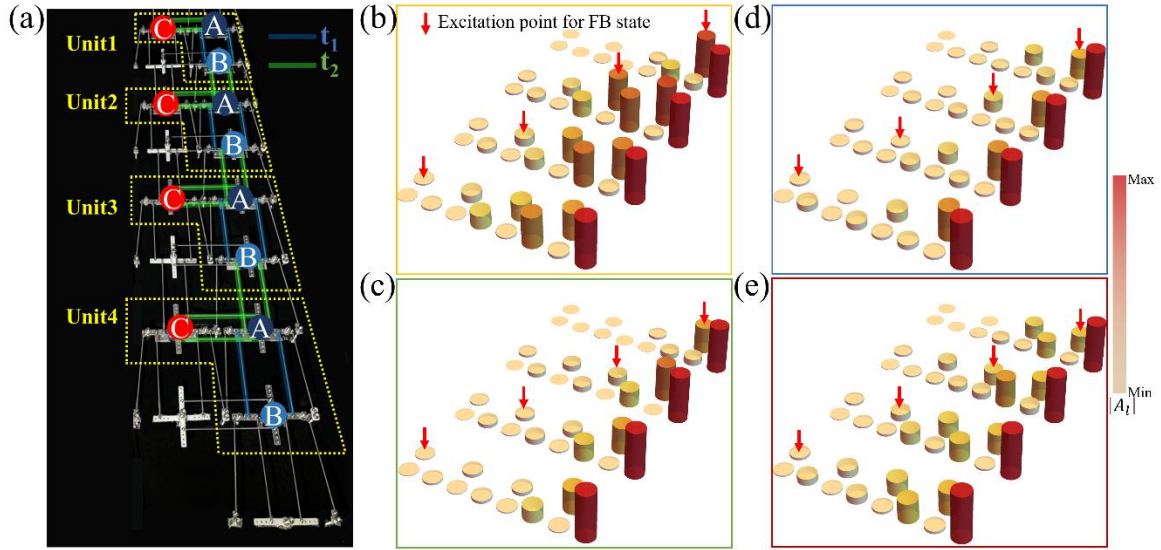


Fig.3 Experimental observation for ESE near the EP points of the non-Hermitian parameter space in a 4 unit-cell elastic wave system. (a) The experimental set up of the 4 unit-cell elastic wave system, yellow dashed boxes marking unit cells 1-4, blue and green lines denoting constant couplings t_1 and t_2 induced by springs connecting different sites, colored circles denoting different sites A, B, and C included in each unit cell. The experimentally measured flat-band states around EP points marked by stars with different colors in Fig. 1,2: (b) $\gamma_1 = 1,52, \gamma_2 = 2,28$ (yellow framed); (c) $\gamma_1 = 1,52, \gamma_2 = 1,99$ (green framed); (d) $\gamma_1 = 1,52, \gamma_2 = 1,57$ (blue framed) and (e) $\gamma_1 = 1,52, \gamma_2 = 1,20$ (red framed). Red arrows denote the excitation point. All flat-band states exhibit ESE induced by dispersive bands' NHSE and flat band-dispersive band hybridization, yet the distribution profiles are different for varied non-Hermitian parameters.

Excite the flat-band states at different unit-cells as marked by the red arrows, the excited flat-band modes are all influenced by the hybridization with their dispersive-band counterparts, thus form ESE; yet for different EPs possessing different non-Hermitian parameters, the measured distribution profiles of ESE are different [Fig.3 (b-e)], possessing different exponential decaying parameters towards the other side of the 1D chain, which consist well with the theoretical predictions [Fig.2 (e)]. These experimental results provide a compelling proof of our inference that the ESE observed on the flat band are induced by the forming of EPs and hybridization with the dispersive bands [See Section 4 of SI for time-evolution data].

We further conduct the experiment in a larger system consisting of 12 unit-cells [Fig.4 (a)] to observe the flat-band ESE at a point away from EP yet still falling in the PBC gap-closed area in the non-Hermitian parameter space. Set the total evolution time to be $t_{\text{tot}} = 20\text{s}$. Starting from the Hermitian point ($\gamma_1 = \gamma_2 = 0$), the properties of the flat-band are clearly seen as shown in the left panel of Fig.4 (b): the centre frequencies of the excited states are all identical at $f_0 = 10.6\text{Hz}$ with a maximum deviation of $\pm 0.06\text{Hz}$ (0.57% for the base frequency). The excited flat-band states in different unit cells are initially localized as shown in the middle panel of Fig.4 (b), which corresponds to the Anderson localization on a normal flat band. Then, to presume adiabatic approximation, the non-Hermitian parameters are dynamically modulated as:

$$\begin{aligned}\gamma_1 &= 1.52 * \text{Sin}\left[\frac{20(t-2*t_{\text{tot}}/5)\pi}{2*t_{\text{tot}}}\right] \\ \gamma_2 &= 2 * \text{Sin}\left[\frac{20(t-2*t_{\text{tot}}/5)\pi}{2*t_{\text{tot}}}\right]\end{aligned}\quad (8)$$

where the dynamics are also governed by the time-dependent Schrödinger equation $H(t)|\psi_n(t)\rangle = \varepsilon_n(t)|\psi_n(t)\rangle$. During this process, the excited flat-band modes start to be influenced by the NHSE of their dispersive-band counterparts as the gap closes thus the dispersive bands begin to hybridize with the flat band, and after the parameters are stable at $\gamma_1 = 1.52, \gamma_2 = 2$, the flat-band eigen states are observed to exhibit ESE as observed in the right panel of Fig.4 (b), all localized at the right-hand side, exponential decaying towards the other side of the 1D chain. In this way, the flat-band ESE is experimentally observed in a larger system [See Section 4 in SI for time-evolution data].

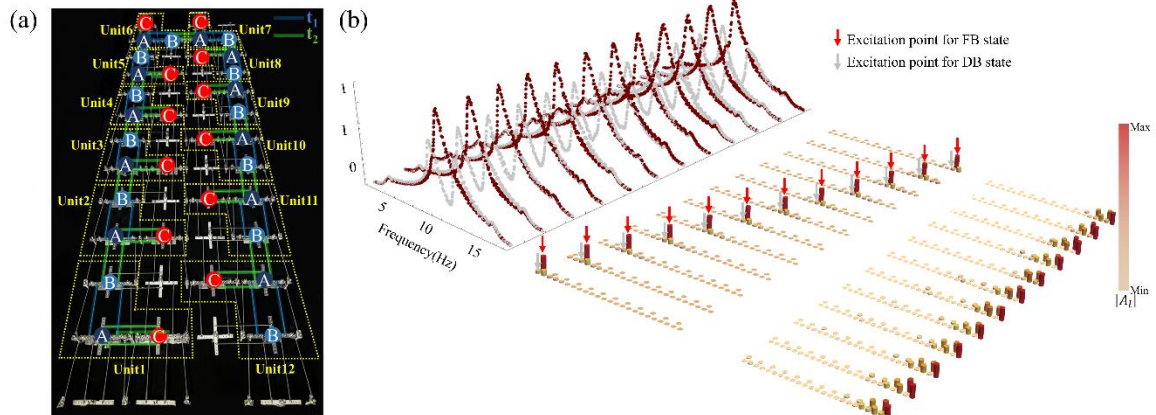


Fig.4 Experimental observation for the time evolution process and ESE on flat band under non-Hermitian conditions in a 12 unit-cell elastic wave system. (a) The experimental set up of the 12 unit-cell elastic wave system, yellow dashed boxes marking unit cells 1-12. (b) The experimental measured results, the left panel demonstrates the spectrum of the flat-band states(red) and dispersive-band states(gray); the middle panel demonstrates the localized states excited at the flat-band frequency for the initial condition(Hermitian), red and gray arrows denoting the excitation points for the flat-band states and dispersive-band states respectively; the right panel demonstrates the flat-band states at the end of the time evolution, all exhibit ESE.

One thing to notice is that, even when the non-Hermitian parameters are increased to larger values outside the gap-closed area, the excited states on the flat band would stay localized [See Section 5 in SI for details]. Thus, through experimental observations of flat-band ESE in different-size systems, we verify that the ESE observed on the flat band are induced by the forming of EPs and hybridization with the dispersive bands, and can exhibit different wave function profiles due to the variation of dispersive-band NHSE.

Conclusions

To conclude, in the gap-closed area for symmetry-protected flat band systems, though the Bloch energy spectrum of the flat band remains as one single dot, with the hybridization between flat band and dispersive bands, the flat-band eigen states can still exhibit a special kind of NHSE when the dot is surrounded by the dispersive-band loop on the complex energy plane, which we call ESE. With analytical analysis, the process of flat band forming EPs with different pairs of dispersive bands in sequence thus experience ESEs with different profiles is clearly demonstrated. With further time-evolution experiments, we eventually verify the generation of flat-band ESE in the specific gap-closed area, the distribution profiles of which can be modulated by different non-Hermitian parameters within the area and the NHSE of their dispersive-band counterparts hybridizing with them. The special type of EPs formed together by dispersive and flat-band states and the flat-band ESE generated correspondingly due to dispersive-flat band hybridization discovered and validated in this work might be beneficial for both future researches on flat-band non-Hermitian physics and real applications.

1. Altmann, S. L. *Band Theory of Solids an Introduction from the Point of View of Symmetry*. (Oxford University Press, 1991).

2. Derzhko, O., Richter, J. & Maksymenko, M. Strongly correlated flat-band systems: The route from Heisenberg spins to Hubbard electrons. *Int. J. Mod. Phys. B* **29**, 1530007 (2015).
3. Tian, H. *et al.* Evidence for Dirac flat band superconductivity enabled by quantum geometry. *Nature* **614**, 440–444 (2023).
4. Törmä, P., Peotta, S. & Bernevig, B. A. Superconductivity, superfluidity and quantum geometry in twisted multilayer systems. *Nat. Rev. Phys.* **4**, 528–542 (2022).
5. Balents, L., Dean, C. R., Efetov, D. K. & Young, A. F. Superconductivity and strong correlations in moiré flat bands. *Nat. Phys.* **16**, 725–733 (2020).
6. Baba, T. Slow light in photonic crystals. *Nat. Photonics* **2**, 465–473 (2008).
7. Song, L. *et al.* Topological Flatband Loop States in Fractal-Like Photonic Lattices. *Laser Photonics Rev.* **17**, 2200315 (2023).
8. Tang, L. *et al.* Photonic flat-band lattices and unconventional light localization. *Nanophotonics* **9**, 1161–1176 (2020).
9. Xu, C. *et al.* Design of full-k-space flat bands in photonic crystals beyond the tight-binding picture. *Sci. Rep.* **5**, 18181 (2015).
10. Leykam, D., Andreanov, A. & Flach, S. Artificial flat band systems: from lattice models to experiments. *Adv. Phys. X* **3**, 1473052 (2018).
11. Bergholtz, E. J. & Liu, Z. Topological Flat Band Models and Fractional Chern Insulators. *Int. J. Mod. Phys. B* **27**, 1330017 (2013).
12. Călugăru, D. *et al.* General construction and topological classification of crystalline flat bands. *Nat. Phys.* **18**, 185–189 (2022).

13. Chalker, J. T., Pickles, T. S. & Shukla, P. Anderson localization in tight-binding models with flat bands. *Phys. Rev. B* **82**, 104209 (2010).
14. Chen, Y., Huang, J., Jiang, K. & Hu, J. Decoding flat bands from compact localized states. *Sci. Bull.* **68**, 3165–3171 (2023).
15. Flach, S., Leykam, D., Bodyfelt, J. D., Matthies, P. & Desyatnikov, A. S. Detangling flat bands into Fano lattices. *EPL Europhys. Lett.* **105**, 30001 (2014).
16. Wang, K., Dutt, A., Wojcik, C. C. & Fan, S. Topological complex-energy braiding of non-Hermitian bands. *Nature* **598**, 59–64 (2021).
17. Noh, J. *et al.* Braiding photonic topological zero modes. *Nat. Phys.* **16**, 989–993 (2020).
18. Barlas, Y. & Prodan, E. Topological Braiding of Non-Abelian Midgap Defects in Classical Metamaterials. *Phys. Rev. Lett.* **124**, 146801 (2020).
19. You, O. *et al.* Observation of Non-Abelian Thouless Pump. *Phys. Rev. Lett.* **128**, 244302 (2022).
20. Citro, R. & Aidelsburger, M. Thouless pumping and topology. *Nat. Rev. Phys.* **5**, 87–101 (2023).
21. Google Quantum AI and Collaborators *et al.* Non-Abelian braiding of graph vertices in a superconducting processor. *Nature* **618**, 264–269 (2023).
22. Iadecola, T., Schuster, T. & Chamon, C. Non-Abelian Braiding of Light. *Phys. Rev. Lett.* **117**, 073901 (2016).
23. Zhang, X.-L. *et al.* Non-Abelian braiding on photonic chips. *Nat. Photonics* **16**, 390–395 (2022).
24. Ashida, Y., Gong, Z. & Ueda, M. Non-Hermitian physics. *Adv. Phys.* **69**, 249–435 (2020).

25. Hu, Y.-M. & Wang, Z. Green's functions of multiband non-Hermitian systems. *Phys. Rev. Res.* **5**, 043073 (2023).
26. Song, F., Yao, S. & Wang, Z. Non-Hermitian Topological Invariants in Real Space. *Phys. Rev. Lett.* **123**, 246801 (2019).
27. Tang, W. *et al.* Exceptional nexus with a hybrid topological invariant. *Science* **370**, 1077–1080 (2020).
28. Tang, W., Ding, K. & Ma, G. Realization and topological properties of third-order exceptional lines embedded in exceptional surfaces. *Nat. Commun.* **14**, 6660 (2023).
29. Yang, Z., Schnyder, A. P., Hu, J. & Chiu, C.-K. Fermion Doubling Theorems in Two-Dimensional Non-Hermitian Systems for Fermi Points and Exceptional Points. *Phys. Rev. Lett.* **126**, 086401 (2021).
30. Song, F., Yao, S. & Wang, Z. Non-Hermitian Skin Effect and Chiral Damping in Open Quantum Systems. *Phys. Rev. Lett.* **123**, 170401 (2019).
31. Li, L., Lee, C. H., Mu, S. & Gong, J. Critical non-Hermitian skin effect. *Nat. Commun.* **11**, 5491 (2020).
32. Lin, R., Tai, T., Yang, M., Li, L. & Lee, C. H. Topological Non-Hermitian skin effect. *Front. Phys.* **18**, 53605 (2023).
33. Wang, W., Wang, X. & Ma, G. Non-Hermitian morphing of topological modes. *Nature* **608**, 50–55 (2022).